Combination of Carriers with Complementary Intratumoral Microdistributions of Delivered α-Particles May Realize the Promise for ^{225}Ac in Large, Solid Tumors

Alaina Howe[1], Omkar Bhatavdekar*[1], Dominick Salerno*[1], Anders Josefsson[2], Jesus Pacheco-Torres[2], Zaver M. Bhujwalla[2], Kathleen L. Gabrielson[3], George Sgouros[2], and Stavroula Sofou[1,4]

[1]*Chemical and Biomolecular Engineering, Institute for NanoBioTechnology, Johns Hopkins University, Baltimore, Maryland;* [2]*Russell H. Morgan Department of Radiology and Radiological Science, Johns Hopkins University, Baltimore, Maryland;* [3]*Molecular and Comparative Pathobiology, Johns Hopkins University, Baltimore, Maryland; and* [4]*Sidney Kimmel Comprehensive Cancer Center, Cancer Invasion and Metastasis Program, Department of Oncology, Johns Hopkins University, Baltimore, Maryland*

α-particle radiotherapy has already been shown to be impervious to most resistance mechanisms. However, in established (i.e., large, vascularized) soft-tissue lesions, the diffusion-limited penetration depths of radiolabeled antibodies or nanocarriers (≤50–80 μm) combined with the short range of α-particles (4–5 cell diameters) may result in only partial tumor irradiation, potentially limiting treatment efficacy. To address this challenge, we combined carriers with complementary intratumoral microdistributions of the delivered α-particles. We used the α-particle generator ^{225}Ac, and we combined a tumor-responsive liposome (which, on tumor uptake, releases into the interstitium a highly diffusing form of its radioactive payload [^{225}Ac-DOTA], potentially penetrating the deeper parts of tumors where antibodies do not reach) with a separately administered, less-penetrating radiolabeled antibody (irradiating the tumor perivascular regions where liposome contents clear too quickly). **Methods:** In a murine model with orthotopic human epidermal growth factor receptor 2–positive BT474 breast cancer xenografts, the biodistributions of each carrier were evaluated, and the control of tumor growth was monitored after administration of the same total radioactivity of ^{225}Ac delivered by the ^{225}Ac-DOTA–encapsulating liposomes, by the ^{225}Ac-DOTA-SCN–labeled trastuzumab, and by both carriers at equally split radioactivities. **Results:** Tumor growth was significantly more inhibited when the same total injected radioactivity was divided between the 2 separate carriers than when delivered by either of the carriers alone. The combined carriers enabled more uniform intratumoral microdistributions of α-particles, at a tumor dose that was lower than the dose delivered by the antibody alone. **Conclusion:** This strategy demonstrates that more uniform microdistributions of the delivered α-particles within established solid tumors improve efficacy even at lower tumor doses. Augmentation of antibody-targeted α-particle therapies with tumor-responsive liposomes may address partial tumor irradiation, improving therapeutic effects.

Key Words: ^{225}Ac; liposomes; antibodies; tumor microdistributions

J Nucl Med 2022; 63:1223–1230
DOI: 10.2967/jnumed.121.262992

Metastatic or recurrent solid cancers present an all too common clinical challenge partly due to development of resistance (*1*). Clinical studies with α-particle emitters have sometimes had exceptional outcomes on patients with metastatic prostate cancer resistant to approved options (*2,3*). The promise of α-particles targeted via antibodies against advanced cancers (not limited to prostate cancer) is currently under investigation in clinical studies. An effective and tolerable α-particle–based treatment against established (i.e., large, vascularized) lesions is critical to successfully handling solid-tumor patients with advanced disease that is resistant to established approaches.

α-particle radiotherapy has already been shown, across a diverse panel of tumor cells, to be impervious to most resistance mechanisms in the absence of transport barriers; the cells most resistant to γ-radiation have been reported to be sensitive to α-particles (*4*). The complexity and level of double-strand DNA damage caused by only a few tracks of α-particles across the cell nucleus overwhelm cellular repair mechanisms mostly independently of the cell oxygenation state and cell cycle (*5*); this inability to repair lethal damage is the reason that α-particle therapy, if optimally delivered, is impervious to resistance. However, the short range of α-particles (40–100 μm), which is ideal for localized irradiation and minimal irradiation of surrounding healthy tissues, also limits penetration within large tumors; the diffusion-limited penetration depths (≤50–80 μm) of established and alternative vectors, such as radiolabeled antibodies or nanocarriers, respectively, combined with the short range of α-particles may result in only partial tumor irradiation (*6*). Importantly, partial tumor irradiation may limit the efficacy of α-particle therapies irrespective of any augmenting bystander effects (*7*).

Tumor-selective delivery strategies for α-particle therapies that aim to spread the intratumoral α-particle distributions over larger regions within solid tumors, and to prolong exposure of cancer cells to delivered radiotherapeutics, may improve efficacy against established tumors. Toward this goal, we evaluated a strategy to deliver the α-particle generator ^{225}Ac as uniformly as possible throughout established tumors using a human epidermal growth factor receptor 2 (HER2)–positive human breast cancer, chosen as a model tumor for proof of concept. We combined 2 different delivery carriers of ^{225}Ac, tumor-responsive liposomes and HER2-targeting antibodies, each administered separately. The liposomes were engineered to have 2 key properties for the implementation of our strategy: the

Received Aug. 2, 2021; revision accepted Nov. 9, 2021.
For correspondence or reprints, contact Stavroula Sofou (ssofou1@jhu.edu).
*Contributed equally to this work.
Published online Nov. 18, 2021.

first is to clear slowly from tumors, and the second is—only in the tumor interstitium—to release highly diffusing forms (because of their small size) of the α-particle emitters (^{225}Ac-DOTA), which then may penetrate the deep parts of tumors where antibodies do not reach (*6*). The antibodies were also labeled with ^{225}Ac, which they deliver mostly closer to the tumor periphery (the perivascular regions), where the liposome-based modality suffers from fast clearance of released therapeutic agents (*8*).

The tumor-responsive liposomes were designed to exhibit the following properties, all of which were triggered by the slightly acidic pH in the tumor interstitium (extracellular pH [pH_e], ~6.7–6.5) (*9*): adherence to the tumor's extracellular matrix (resulting in slower liposome clearance from the tumor (*8*)), low uptake or internalization by cancer cells (*8*), and release of contents directly into the interstitium as triggered by the tumor acidity (*6*). The HER2-targeting antibody trastuzumab, which was administered separately from liposomes, was chosen because of its high affinity for the HER2 receptor, reasonable radiolabeling, and well characterized in vivo behavior.

Here, we evaluate our hypothesis that combination of different carriers delivering α-particle radiotherapies to complementary regions of the same solid tumor results in more uniform irradiation over a larger fraction of the solid tumor's volume and, therefore, in greater inhibition of tumor growth than occurs with the same administered radioactivity delivered by each carrier alone.

MATERIALS AND METHODS

Materials

All materials are described in the supplemental section (available at http://jnm.snmjournals.org). ^{225}Ac (actinium chloride) was supplied by the U.S. Department of Energy Isotope Program, managed by the Office of Isotope R&D and Production.

Liposome Formation and Characterization

Tumor-responsive liposomes, composed of 20PC:DPPS:cholesterol:DSPE-polyethylene glycol-diammonium phosphate:DPPE-rhodamine at a 0.61:0.26:0.04:0.09:0.001 molar ratio, were formed using the thin-film hydration method as described in detail in the supplemental section (*6*). Liposomes were characterized for size and ζ-potential using a Zetasizer NanoZS90 (Malvern).

Radiolabeling of Carriers with ^{225}Ac/^{111}In

DOTA-SCN-trastuzumab (or diethylenetriaminepentaacetic acid [DTPA]-SCN-trastuzumab) was radiolabeled and characterized as described in the supplemental section (*6*). Liposomes encapsulating DOTA (or DTPA) were loaded with ^{225}Ac (or ^{111}In) using the ionophore A23187 (*6*).

Cell Culture

BT474 and the trastuzumab-resistant BT474 (BT474_R) were obtained from American Type Culture Collection and grown in treated cell culture flasks at 37°C and 5% CO_2 in Hybri-Care medium (American Type Culture Collection) buffered with sodium bicarbonate supplemented with 10% fetal bovine serum, penicillin (100 U/mL), and streptomycin (100 mg/mL).

Clonogenic Survival

After incubation of cell monolayers for 6 h with varying concentrations of radioactivity, the cells were washed and plated in dishes to grow until formation of colonies, as described in detail in the supplemental section.

TABLE 1
Characterization of Tumor-Responsive Liposomes Loaded with ^{225}Ac-DOTA

Size (nm)	ζ-potential (mV)			% loading	Specific activity* (MBq/μmol of lipid)	Retention kinetics ($y = y\infty + a \times e^{-bt}$)				
	pH 7.4	pH 6.5	pH 6.0			pH	$y\infty$ (%)	a (%)	b (1/h)	$t^1/_2$ (h)
118 ± 15 (polydispersity index, 0.099 ± 0.051) (n = 15)	−1.5 ± 1.4† (n = 15)	−0.8 ± 1.2‡ (n = 15)	−0.04 ± 1.1†‡ (n = 15)	51.1 ± 8.6 (n = 15)	0.5 ± 0.2 (n = 9)	7.4	88.8 ± 0.7	10.9 ± 1.2	1.2 ± 0.3	0.6 ± 0.2
						7.0	84.9 ± 1.3	13.8 ± 1.7	0.5 ± 0.1	1.4 ± 0.1
						6.5	77.8 ± 1.2	21.2 ± 1.5	0.4 ± 0.1	1.7 ± 0.1
						6.0	72.4 ± 0.7	27.8 ± 1.0	0.7 ± 0.1	1.0 ± 0.0

*Starting activity, 1.5–3.7 MBq.
†$0.001 < P < 0.01$.
‡$P < 0.001$.
$t^1/_2$ = half-time.

TABLE 2
Characterization of ^{225}Ac-Labeled HER2-Targeting Trastuzumab

Radiolabeling efficiency (%)	Immunoreactivity (%)	Specific activity* (MBq/mg of antibody)	Radiochemical purity	24-h retention (%)	K_D (nM)	
					BT474	BT474_R
53.8 ± 11.4 (n = 14)	95.9 ± 1.4 (n = 14)	3.4 ± 0.7 (n = 11)	97.8 ± 1.8 (n = 14)	90.6 ± 2.5 (n = 14)	24.6 ± 4.9	10.2 ± 1.7

*Starting activity, 0.4–1.1 MBq
K_D = dissociation constant.

Spheroid Formation and Spatiotemporal Profiles

BT474 cells were seeded on poly-2-hydroxyethyl methacrylate–coated, round-bottomed 96-well plates; were centrifuged; and were allowed to grow to the reported size before initiation of treatment (*6*). Spheroids were incubated with fluorescently labeled liposomes or antibody for 6 or 24 h, respectively, to scale with their corresponding blood circulation times. As described in the supplemental section (*8*), at different times spheroids were sampled and sliced, and the equatorial section was imaged using fluorescence microscopy. The spatial profiles (radial concentrations) were evaluated using an in-house eroding code to determine the average fluorescence intensity of each 5-μm concentric ring on the spheroids' sections. The spatial distributions at each time point were integrated (using the trapezoid rule) to evaluate the time-integrated concentration versus radius.

Spheroid Growth and Outgrowth Studies

Spheroids were incubated for 6 h with ^{225}Ac-DOTA–loaded liposomes (1 mM total lipid) or 24 h with ^{225}Ac-DOTA-SCN-trastuzumab (10 μg/mL). On completion of incubation, spheroids were transferred to fresh medium and the spheroid volume was monitored until the nontreated spheroids stopped growing (17 d later), at which point spheroids were individually plated on cell culture-treated, flat-bottomed 96-well plates and allowed to grow. The number of live cells per well was reported as percentage outgrowth relative to the numbers of live cells that received no treatment, when the latter reached confluency.

Animal Studies

One million BT474 cells suspended in 100 μL of 50:50 v:v Matrigel (Corning Life Sciences):serum-free Hybri-Care medium were inoculated into the second mammary fat pad of 5- to 6-wk-old NCR-nu/nu female mice (Taconic) at 24 h after subcutaneous implantation of a 17β-estradiol (1.7 mg) + progesterone (10 mg) hormone pellet (Innovative Research of America).

On tumors reaching 50 mm^3, mice were randomly assigned to a group. For biodistribution studies, the animals were intravenously administered (352–444 kBq/animal) ^{111}In-DTPA-encapsulating liposomes or ^{111}In-DTPA-SCN-trastuzumab in 0.1 mL, and at different time points the animals were sacrificed and their organs weighed and measured for radioactivity.

In addition to the cold conditions and to no treatment, for treatment studies the mice were administered a single 0.1-mL intravenous injection of 4.625 kBq or 9.25 kBq of ^{225}Ac-DOTA-SCN-trastuzumab, ^{225}Ac-DOTA-loaded liposomes, or a combination of the two at a constant total administered radioactivity. The total mass of antibody was kept constant at 15 μg/mouse. Every other day, the mice were weighed and their tumor volumes measured with a digital caliper (resolution, 0.01 mm). Histopathologic analysis of all organs and tumors was performed on hematoxylin- and eosin-stained sections on day 24 after initiation of therapy.

α-Camera Imaging

Tumor-bearing mice were injected intravenously with ^{225}Ac-DOTA-SCN-trastuzumab, ^{225}Ac-DOTA-loaded liposomes, or both at 148 kBq of total radioactivity and were sacrificed 24 h later. Tumor and tissues were immediately harvested and sliced. The exposure time for the α-camera was 24 h per sample (*10*), and the images were analyzed using ImageJ, version 1.49b (National Institutes of Health) after being decay-corrected to the time of sacrifice.

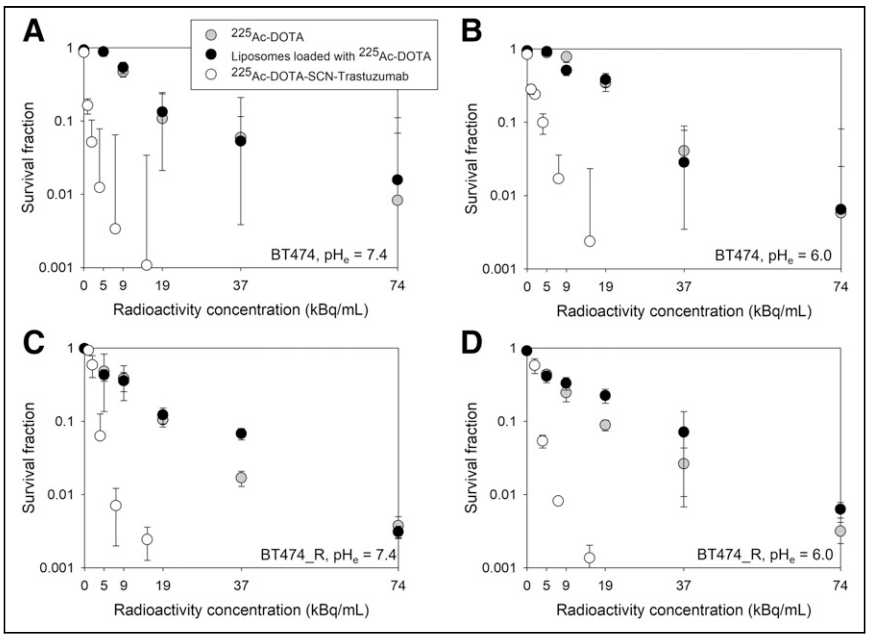

FIGURE 1. Colony survival of trastuzumab-sensitive BT474 (1.50 ± 0.10 × 10^6 HER2 copies per cell) breast cancer cells after 6 h of incubation at 37°C with free ^{225}Ac-DOTA, tumor-responsive liposomes loaded with ^{225}Ac-DOTA, and radiolabeled trastuzumab (^{225}Ac-DOTA-SCN-Ab) at extracellular pH of 7.4 (A and C) or 6.0 (B and D), as lowest expected acidic value of tumor interstitial pH_e. Radiolabeled trastuzumab's specific activity was 2.9 MBq/mg at highest radioactivity concentration. Cold conditions of liposomes and antibody are indicated at zero radioactivity concentration. Error bars correspond to SD of repeated measurements (4–6 samples per radioactivity concentration).

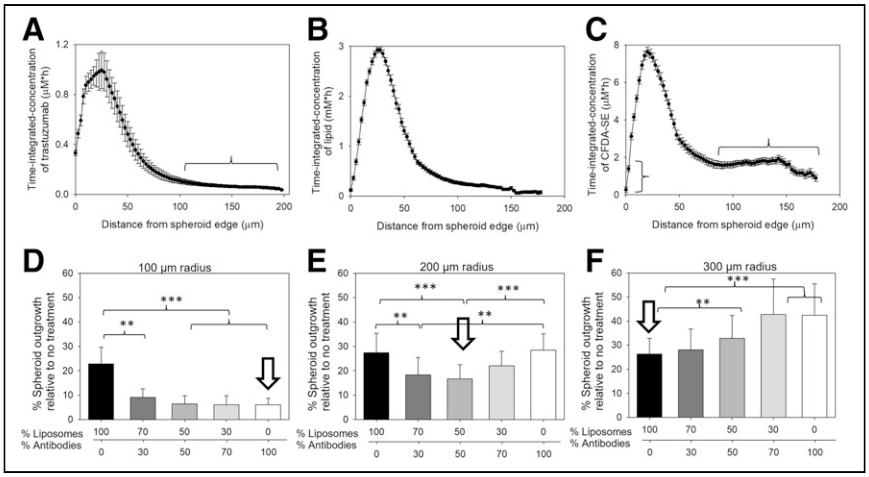

FIGURE 2. (A–C) Time-integrated concentrations in HER2-positive BT474 spheroids (r = 200 μm) of fluorescently labeled antibody (AlexaFluor-647-NHS-trastuzumab) used as surrogate of ^{225}Ac-DOTA-SCN-trastuzumab (A; horizontal bracket indicates <10% of peak value at distances beyond 100 μm from edge), lipids (DPPE-rhodamine-labeled liposomes; vertical bracket indicates too-rapid clearance of released fluorophore close to spheroid edge) (B), and carboxyfluorescein diacetate succinimidyl ester (CFDA-SE) fluorophores (used as surrogates of ^{225}Ac-DOTA) (C; horizontal bracket indicates uniform time-integrated values at ~25% of peak value) delivered by tumor-responsive liposomes. Spatial distributions obtained at different time points (during carrier uptake by and clearance from spheroids) were integrated using trapezoid rule along spheroid radius. Error bars correspond to propagated SD of measurements of 3–6 equatorial spheroid sections per time point. Immunoreactivity of fluorescently labeled antibody was 88.2% ± 2.7%. (D–F) Greatest suppression of extent of outgrowth (used as indirect surrogate of tumor recurrence) by carrier, or combinations of carriers, of ^{225}Ac depends on spheroid size (representing tumor-avascular regions). Outgrowth control was best enabled (indicated by arrow) for small spheroids (radius, 100 μm) by radiolabeled antibodies (^{225}Ac-DOTA-SCN-trastuzumab) (D), for large spheroids (radius, 300 μm) by tumor-responsive liposomes encapsulating ^{225}Ac-DOTA (F), and for medium spheroids (radius, 200 μm) by dividing same total radioactivity between both carriers (E). Total radioactivity concentration was kept constant per spheroid size: 9.25 kBq/mL (D), 13.75 kBq/mL (E), and 18.5 kBq/mL (F). Error bars correspond to SD of repeated measurements (4–5 spheroids per condition, 2 independent preparations). **0.001 < P < 0.01. ***P < 0.001.

MRI for Evaluation of Tumor pH_e

Briefly, the animals were injected intraperitoneally with the pH_e probe (±)2-(imidazol-1-yl)succinic acid (ISUCA), and anatomic T2-weighted spin-echo images were acquired using rapid-acquisition relaxation enhancement on a Bruker BioSpec 9.4-T horizontal MRI scanner. pH_e was determined as described in the supplemental section (*11*).

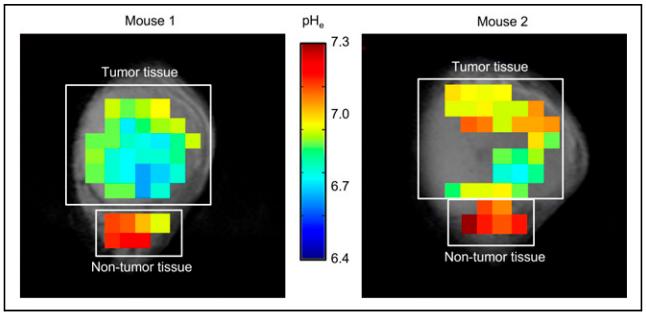

FIGURE 3. Tumor and nontumor pH_e maps of 2 different NCR nu/nu female mice with orthotopic BT474 xenografts that were intraperitoneally administered ISUCA and imaged by spectroscopic MRI. pH_e maps are overlaid with anatomic MR images of tumors. ISUCA chemical shift for each voxel (1 × 1 × 4 mm) of acquired multivoxel spectroscopy grid was transformed into pH value using Henderson–Hasselbalch calibration curve and presented as colored pH_e map.

Dosimetry

Dosimetry was performed following a previously described methodology (*12,13*) using the software package 3D-RD-S (Radiopharmaceutical Imaging and Dosimetry, LLC), based on the biodistributions of ^{111}In-labeled liposomes (Supplemental Tables 1 and 2; Supplemental Fig. 1) or of the radiolabeled antibody (as described previously (*14*)). ^{111}In has been confirmed as a surrogate of ^{225}Ac biodistribution (Supplemental Fig. 2 (*14*)). The longest-lived ^{225}Ac daughter, ^{213}Bi, for the non–cell-internalizing liposomes, unlike for the cell-internalizing trastuzumab, was estimated to partly (25%) translocate from the site of the original parent decay (*13*).

Statistical Analysis

Results are reported as the arithmetic mean of n independent measurements ± SD. Significance in multiple comparisons and pair comparisons was evaluated by 1-way ANOVA and unpaired Student t testing, respectively, with P values of 0.05 considered to be significant.

RESULTS

Carrier Characterization

Table 1 shows the change in the liposomes' apparent ζ-potential toward less negative values with lowering pH; this change was partly attributed to protonation of diammonium phosphate on the adhesion lipid, with an apparent value of 6.8 for negative log of the acid dissociation constant (*8*). Acidification also resulted in release of encapsulated ^{225}Ac-DOTA from liposomes (Supplemental Fig. 3). The radiolabeled trastuzumab is characterized in Table 2 and Supplemental Figure 4.

Survival Assay on Cell Monolayers

Both cell lines, in monolayers, exhibited the same sensitivity to free ^{225}Ac-DOTA and to ^{225}Ac-DOTA–encapsulating liposomes, independently of pH (Fig. 1; Supplemental Fig. 5), since liposomes were designed to minimally associate with cancer cells (*8*), as is also the case for free ^{225}Ac-DOTA. Both cell lines exhibited comparable survival responses to ^{225}Ac-DOTA-SCN-trastuzumab, demonstrating lack of resistance to α-particles independently of the reported resistance to trastuzumab for BT474_R. The HER2 expression by the 2 cell lines was comparable (1.5×10^6 vs. 0.93×10^6 copies per cell, Supplemental Fig. 4).

Spheroids: Spatiotemporal Microdistributions and Response to Delivered ^{225}Ac

The time-integrated microdistributions of trastuzumab in spheroids (Fig. 2A), used as surrogates of tumor-avascular regions, exhibited high accumulation within only the first 60 μm from the spheroid edge, with less than 10% of the peak value at distances beyond 100 μm from the edge. As expected, liposomes did not penetrate the spheroids' longer distances than the antibody (Fig. 2B). Conversely, at distances of 80 μm from the spheroid edge and beyond, the fluorophore (Fig. 2C), which was used as a drug surrogate and was released from the liposomes, exhibited uniform

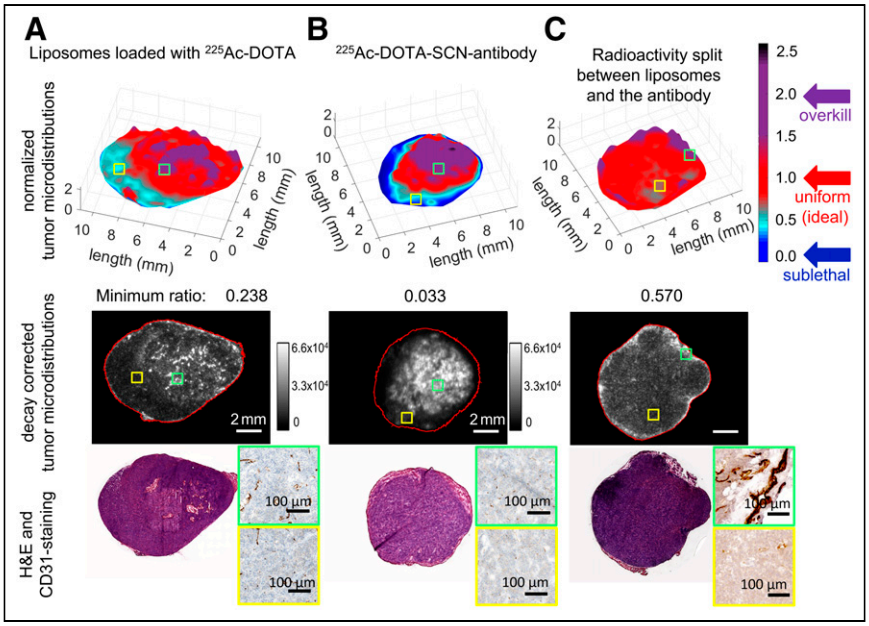

FIGURE 4. Microdistributions of same total radioactivity of ^{225}Ac delivered by tumor-responsive liposomes only (A), radiolabeled trastuzumab only (B), and both liposomes and—separately administered—trastuzumab (C) on tumor sections harvested 24 h after intravenous administration of 148 kBq per animal. High-radioactivity relative levels (ratios > 2, purple) were detected in densely vascularized tumor areas (CD31+, green insets); low-radioactivity relative levels (ratios < 0.6) were detected in sparsely vascularized areas (yellow insets). (Top panel) Map of normalized pixel intensities (where each pixel intensity was divided by average of intensities over entire tumor section) of ^{225}Ac relative to intensities averaged over entire tumor section so as to evaluate range of heterogeneities in ^{225}Ac microdistributions. Regions in red (with ratios around unity) indicate local distributions close to mean radioactivities delivered to tumor. Regions in cyan and dark blue (with normalized pixel intensity ratios well below mean radioactivities delivered to tumor) indicate regions with low or too-low radioactivities relative to tumor mean, expected to result in less cell killing. Regions in purple are where significantly more than tumor-averaged radioactivity is delivered. (Middle and bottom panels) Decay-corrected α-camera images and hematoxylin- and eosin (H&E)-stained and CD31-stained images of sequential 16-μm-thick tumor sections.

time-integrated values at approximately 25% of peak value. However, close to the spheroid edge, the released fluorophore cleared too rapidly from the spheroid. The acidification of the spheroids' interstitial pH (pH_e), which triggers the properties of liposome adhesion and content release, ranged from 7.4 close to the spheroid edge to around 6.5 at the spheroid center (Supplemental Fig. 6). The time-integrated microdistributions in Figure 2 reflect the microdosimetry of the delivered ^{225}Ac but not of the radioactive daughters.

After exposure to ^{225}Ac, divided between liposomes and the antibody, the carrier resulting in greatest suppression of spheroid outgrowth depended on the spheroid size at the time of treatment. On small spheroids (100-μm radius), delivery of radioactivity by the targeting antibody (Fig. 2D) was most efficient. The heterogeneous distribution of trastuzumab (high uptake but localized mostly close to the spheroid edge, Fig. 2A) did not impact efficacy because the longest spheroid distance (100-μm radius) was comparable to the range of α-particles in tissue (≤100 μm) (*6*). On large spheroids (300-μm radius, corresponding to avascular distances almost 3 times longer than the range of α-particles in tissue), delivery of radioactivity by liposomes (that released ^{225}Ac-DOTA into the interstitium) was most efficient; this efficiency was attributed to the deeper penetration (as supported by the fluorescent surrogate in Fig. 2C) of released ^{225}Ac-DOTA toward the spheroid center (*6*). In spheroids with an intermediate size (200-μm radius), the combination of the 2 carriers resulted in a better cell kill.

Tumor and Tissue pH_e Measurement

The MR images in Figure 3 showed that there was measurable acidity in the tumor interstitium and that the microdistributions of interstitial pH_e tumor maps were not uniform; indeed, they varied across tumors from different animals. Importantly, the pH_e values measured were close to the acidic values that trigger the release and adhesion properties on liposomes.

In Vivo Assessment

In agreement with the profiles of delivered microdistributions of therapeutics in spheroids (Fig. 2), the tumor microdistributions of radioactivity in vivo were more uniform when delivered by both carriers than when delivered by each carrier alone. In particular, the normalized microdistributions of ^{225}Ac in tumor sections were more heterogeneous when the entire radioactivity was delivered by each carrier alone (Figs. 4A and 4B) than when split between the 2 carriers (Fig. 4C). Importantly, in both tumor sections where ^{225}Ac was delivered by only a single carrier, areas with low and too-low delivered radioactivities occupied significant fractions; regions that were too low were well below the mean tumor-delivered values and, therefore, could result in a lower cell kill. In densely vascularized areas (CD31-positive areas) the delivered normalized radioactivity levels were closer to and above unity (levels ranged from ideal to overkill), whereas in sparsely vascularized areas the levels ranged from sublethal (for the antibody) to too low (for liposomes) to least low (for the combination).

In agreement with the extent of uniformity in tumor microdistributions of ^{225}Ac, the volume growth of orthotopic BT474 xenografts was inhibited most when radioactivity was delivered by equally splitting the same total radioactivity (9.25 kBq (*6*)) between the 2 carriers (4.62 kBq + 4.62 kBq) that were administered simultaneously, as opposed to administering the same total radioactivity (9.25 kBq) by each carrier alone ($P < 0.001$, Fig. 5A).

The dosimetry in Table 3 shows that the equal radioactivity split between the 2 carriers—which resulted in the best tumor inhibition—delivered less dose to the tumor than when the antibody alone was used, underscoring the significance of α-particle microdistributions within the tumors. Individual growth plots for animal tumors are shown in Supplemental Figure 7. The same trend was observed at half the total administered radioactivity (Supplemental Figs. 8 and 9). Table 3 also shows that the carrier combination delivered less dose to the kidneys than did the antibody alone. The delivered dose to the liver by the carrier combination was similar to that delivered by each carrier alone. The error in the calculated dose to the spleen, delivered by the radiolabeled antibody, was large because of poor fitting. For more accurate fitting of the calculated dose to the spleen, sampling at longer time points would be required to capture biologic clearance from the spleen.

Pathologic evaluation of tumors on day 24 demonstrated visibly increased collagen on treatment with ^{225}Ac when delivered by the

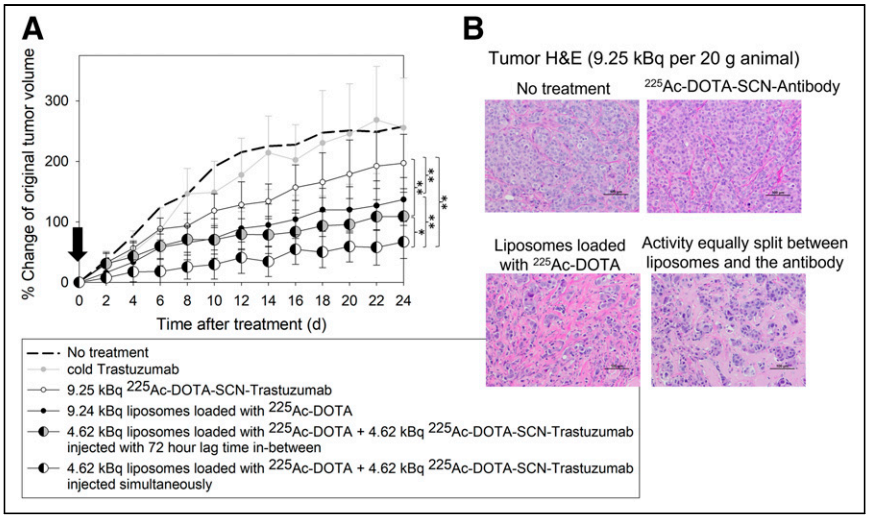

FIGURE 5. (A) Volume progression of HER2-positive BT474 orthotopic xenografts on NCR nu/nu female mice after single intravenous administration (arrow) of 9.25 kBq of ^{225}Ac per 20-g mouse delivered by radiolabeled trastuzumab alone (^{225}Ac-DOTA-SCN-antibody, 2.96 MBq/mg specific radioactivity in injectate); tumor-responsive liposomes loaded with ^{225}Ac-DOTA alone; both carriers at equally split (same total) radioactivity, with radiolabeled antibody being administered 72 h after liposomes (to largely allow for clearance of latter from liver and spleen); and both carriers at equally split (same total) radioactivity injected simultaneously. Data points are mean values of 8–9 animals per group, and error bars are SD. Significance was calculated with 1-way ANOVA ($P < 0.05$). (B) Hematoxylin- and eosin (H&E)-stained tumor sections. Scale bar = 100 μm. *$0.01 < P < 0.05$. **$0.001 < P < 0.01$.

combination of both carriers, compared with either carrier alone (Fig. 5B). Histopathologic analysis showed no noteworthy hepatic, cardiac, or renal toxicities in any construct at the time the animals were killed (Supplemental Fig. 10). Slight inflammation in the diaphragm of the liposome-only treatment group was observed, but otherwise there was no visible lung inflammation. Additionally, increased cell death in and reduced size of the spleen was observed in the liposome-only condition, in agreement with the significant splenic uptake. Long-term renal toxicities (9.5 mo after intravenous injection) of liposomal ^{225}Ac-DOTA at the maximum tolerated dose in tumor-free mice were not detected (*13*). The animal weight during the study did not decrease below 10% of the starting weight (Supplemental Fig. 11).

Survival was not a meaningful endpoint in this study, because tumor growth was estrogen-dependent; tumor growth rates (as shown by the nontreated group, Fig. 5A) reached an asymptote after approximately 60 d from estrogen pellet implantation.

DISCUSSION

We hypothesized that improvement in the spatial uniformity of an α-particle emitter within solid tumors may address the challenge of partial irradiation by α-particles and, therefore, improve efficacy even at lower tumor-absorbed doses. Using a simple and clinically implementable approach, we demonstrated that the spatial intratumoral uniformity of ^{225}Ac can be improved by combinations of 2 separate carriers with complementary tumor microdistributions. Our approach optimized payload delivery, delivering a large number of α-particles at the tumor perivascular regions (via the targeting antibody), where the cell number is greatest and where cells are growing most aggressively, and, simultaneously, a high-capacity penetrating payload to the tumor interior (via the tumor-responsive liposomes), where the dormant and resistant cells are most likely to be responsible for treatment failure (*15*). The same total administered radioactivity was equally divided between the 2 carriers, resulting in synergistic inhibition of tumor growth compared with each carrier alone. It is possible that different radioactivity split ratios between the carriers may result in even better inhibition of tumor growth solely due to more uniform spatiotemporal microdistributions of emitters within tumors.

In contrast to the more homogeneous microdistributions of delivered radioactivity in tumors to improve killing of cancer cells, heterogeneous microdistributions, such as in the liver, could explain the lack of hepatic toxicities on the basis of localized, partial irradiation. Although liver uptake was significant when radioactivity was delivered by liposomes, previous studies at the maximum tolerated dose with liposomes did not reveal any hepatic or splenic toxicities (the main off-target organs) even 9.5 mo after injection (*13*). At least for the liver, one reason the significant delivered doses do not

TABLE 3
Dosimetry Results

	Antibody only		Liposomes only		Same total injected radioactivity equally split between antibody and liposomes	
Tissue	Absorbed dose (Gy)	SD	Absorbed dose (Gy)	SD	Absorbed dose (Gy)	SD
Kidneys	6.25	0.79	0.17	0.07	3.21	0.79
Liver	2.21	1.21	1.08	0.22	1.64	1.23
Lungs	0.94	0.29	0.22	0.21	0.58	0.36
Spleen	9.51	30.60	1.41	0.54	5.46	30.60
Tumor	6.68	1.55	0.40	0.06	3.54	1.55

Dose is mean and SD, not adjusted by relative biological effectiveness.

cause toxicities might be the localized, patchy patterns of liver irradiation (as opposed to the liver's uniform irradiation by the radiolabeled antibody). Radioactivity delivered to the liver by liposomes was strikingly grainy, suggesting heterogeneous or partial irradiation and possibly a limited cell kill (Supplemental Fig. 12). Liposomes are usually sequestered by Kupffer cells, which reside on the luminal side of the liver sinusoids, possibly limiting irradiation of all hepatocytes. Hepatic toxicity was not observed in the present study, in which 63% of the maximum tolerated dose (*6*) was administered. Regarding the spleen, we previously showed that at the maximum tolerated dose of ^{225}Ac delivered by liposomes, the initial splenic moderate-to-high hemosiderin deposition in the red pulp and reduced extramedullary hematopoiesis, observed right after administration of radioactivity, subsided and the spleen fully recovered after 9.5 mo in tumor-free mice (*13*).

Specific to ^{225}Ac are renal toxicities in mice—toxicities that were previously partially connected to escape in the blood of the last radioactive daughter of ^{225}Ac, ^{213}Bi, when ^{225}Ac was delivered by long-circulating carriers, such as antibodies, in addition to antibody renal uptake (*14*). For the ^{225}Ac-encapsulating liposomes, long-term renal toxicities at the maximum tolerated dose were not observed in mice (*13*). In human trials using ^{225}Ac-labeled antibodies or small molecules (*3,16*), renal toxicities have not been reported yet. For liposomes, it would most possibly be the hepatic and splenic uptake that could raise concerns possibly requiring further investigation (*17*).

To potentially mitigate toxicities in the liver and spleen by decreasing the corresponding delivered dose rates, radiolabeled antibodies were administered 72 h after administration of radiolabeled liposomes. In spheroids, the order and lag time ($\leq$72 h) of administering each carrier did not significantly affect inhibition of spheroid outgrowth (Supplemental Fig. 13). In mice, this approach (Fig. 5A) still improved tumor growth inhibition relative to delivering the same total radioactivity by each carrier alone. Alternatively, a strategy that warrants investigation is dose fractionation of the antibody or liposome carriers—a strategy that may provide therapeutic and toxicity advantages. Notably, the presented dosimetry assumed the biologic clearance kinetics of the delivered radionuclides from tissues to be comparable to the half-life of ^{225}Ac. This assumption introduced an uncertainty in the calculated total emitted energies retained by tissues in mice; it is possible that in humans the relative uncertainties are smaller, given that the clearance kinetics of carriers from tissues are known to be slower than in mice.

Two points are key to the clinical relevance and applicability of this approach. The first is the vascular permeability of tumors to the administered liposomes; when human tumors exhibit vascular permeability to liposomes, the extent of liposome uptake by tumors strongly and favorably correlates with tumor response (*17*). The second is the acidification of the intratumoral pH_e, as it relates to triggering the properties of adhesion and release on our liposomes; acidification is common in tumors of patients with breast (and other) cancers (*15*) and correlates with highly aggressive tumors (*9,15,18*), with reported values comparable to the values ($6.60 \leq pH_e \leq 6.98$) required to activate our liposomes. Importantly, in our studies, although the intratumoral acidity was highly variant, the strategy of combining the 2 carriers still resulted in better tumor growth inhibition.

Our delivery approach is aimed at the spatial scale of the avascular tumor regions; these regions are bounded and defined by the distances to the nearest blood vessels within the tumors, and their order of magnitude ranges from a few tenths of a micrometer to possibly several hundredths of a micrometer (*19*). The distances to the nearest blood vessels in tumors are not on the order of magnitude of macroscopic tumor sizes, although they are expected to increase in larger tumors (*19*). From this perspective, the intratumoral microdistributions of α-particle emitters delivered by our strategy would be driven by the distributions of the distances to the nearest blood vessels within tumors and not directly by the macroscopic size of the tumors themselves (*20*).

The spheroids studied here demonstrated the different efficacies of each of the 2 delivery carriers as a function of these distances (Figs. 2D–2F). Effective scaling up of this approach to human tumors will depend not only on the lengths of the distances to the nearest blood vessels (which should be within reach by the released highly diffusing forms of the α-particle emitters) but also, importantly, on the extent of uptake and microdistributions of the radioactivity in off-target organs such as the liver. The potential for successful scaling up of this approach to humans will be determined by our ability to optimize the radioactivity microdistributions until they are as uniform as possible within the tumor (for maximum killing efficacy) and as heterogeneous as possible within the off-target normal organs (for minimum toxicities), as we show is the case in mouse liver for radioactivity delivered by liposomes (Supplemental Fig. 12).

CONCLUSION

This study showed that there is potential to expand the impact of α-particle therapies on established solid tumors by choosing combinations of carriers based on the complementarity of the intratumoral microdistributions of the delivered α-particle emitters while maintaining the same administered radioactivities.

DISCLOSURE

This work was partially supported by a grant from the Elsa U. Pardee Foundation, by American Cancer Society Research Scholar Grant RSG-12-044-01, by National Science Foundation grant CBET1510015, and by the Under Armour Innovation Award. No other potential conflict of interest relevant to this article was reported.

KEY POINTS

QUESTION: Can the partial irradiation of solid tumors by α-particles, delivered with traditional radionuclide carriers, be rectified to improve efficacy?

PERTINENT FINDINGS: The partial irradiation of solid tumors by α-particle emitters can be rectified by combining carriers with complementary intratumoral microdistributions of the delivered α-particle emitters.

IMPLICATIONS FOR PATIENT CARE: Combination of separate carriers with complementary intratumoral microdistributions of α-particle emitters (^{225}Ac in this study) could be a general strategy to control solid tumor growth both in preclinical investigations and in the design of personalized α-particle therapies for patients.

REFERENCES

1. Cancer facts and statistics. American Cancer Society website. https://www.cancer.org/research/cancer-facts-statistics.html. Accessed May 4, 2022.

2. Kratochwil C, Bruchertseifer F, Giesel FL, et al. ^{225}Ac-PSMA-617 for PSMA-targeted α-radiation therapy of metastatic castration-resistant prostate cancer. *J Nucl Med.* 2016;57:1941–1944.
3. Kratochwil C, Haberkorn U, Giesel FL. ^{225}Ac-PSMA-617 for therapy of prostate cancer. *Semin Nucl Med.* 2020;50:133–140.
4. Yard BD, Gopal P, Bannik K, Siemeister G, Hagemann UB, Abazeed ME. Cellular and genetic determinants of the sensitivity of cancer to α-particle irradiation. *Cancer Res.* 2019;79:5640–5651.
5. McDevitt MR, Sgouros G, Sofou S. Targeted and nontargeted α-particle therapies. *Annu Rev Biomed Eng.* 2018;20:73–93.
6. Zhu C, Sempkowski M, Holleran T, et al. Alpha-particle radiotherapy: for large solid tumors diffusion trumps targeting. *Biomaterials.* 2017;130:67–75.
7. Wang R, Coderre JA. A bystander effect in alpha-particle irradiations of human prostate tumor cells. *Radiat Res.* 2005;164:711–722.
8. Stras S, Howe A, Prasad A, Salerno D, Bhatavdekar O, Sofou S. Growth of metastatic triple-negative breast cancer is inhibited by deep tumor-penetrating and slow tumor-clearing chemotherapy: the case of tumor-adhering liposomes with interstitial drug release. *Mol Pharm.* 2020;17:118–131.
9. Vaupel P, Kallinowski F, Okunieff P. Blood flow, oxygen and nutrient supply, and metabolic microenvironment of human tumors: a review. *Cancer Res.* 1989;49:6449–6465.
10. Bäck T, Jacobsson L. The alpha-camera: a quantitative digital autoradiography technique using a charge-coupled device for ex vivo high-resolution bioimaging of α-particles. *J Nucl Med.* 2010;51:1616–1623.
11. Pacheco-Torres J, Mukherjee N, Walko M, et al. Image guided drug release from pH-sensitive ion channel-functionalized stealth liposomes into an in vivo glioblastoma model. *Nanomedicine.* 2015;11:1345–1354.
12. Sgouros G, Roeske JC, McDevitt MR, et al; SNM MIRD Committee. MIRD pamphlet no. 22 (abridged): radiobiology and dosimetry of alpha-particle emitters for targeted radionuclide therapy. *J Nucl Med.* 2010;51:311–328.
13. Prasad A, Nair R, Bhatavdekar O, et al. Transport-driven engineering of liposomes for delivery of α-particle radiotherapy to solid tumors: effect on inhibition of tumor progression and onset delay of spontaneous metastases. *Eur J Nucl Med Mol Imaging.* 2021;48:4246–4258.
14. Song H, Hobbs RF, Vajravelu R, et al. Radioimmunotherapy of breast cancer metastases with alpha-particle emitter ^{225}Ac: comparing efficacy with ^{213}Bi and ^{90}Y. *Cancer Res.* 2009;69:8941–8948.
15. Vaupel P. Tumor microenvironmental physiology and its implications for radiation oncology. *Semin Radiat Oncol.* 2004;14:198–206.
16. Jurcic JG. Targeted alpha-particle therapy for hematologic malignancies. *Semin Nucl Med.* 2020;50:152–161.
17. Lee H, Shields AF, Siegel BA, et al. ^{64}Cu-MM-302 positron emission tomography quantifies variability of enhanced permeability and retention of nanoparticles in relation to treatment response in patients with metastatic breast cancer. *Clin Cancer Res.* 2017;23:4190–4202.
18. Estrella V, Chen T, Lloyd M, et al. Acidity generated by the tumor microenvironment drives local invasion. *Cancer Res.* 2013;73:1524–1535.
19. Lauk S, Zietman A, Skates S, Fabian R, Suit HD. Comparative morphometric study of tumor vasculature in human squamous cell carcinomas and their xenotransplants in athymic nude mice. *Cancer Res.* 1989;49:4557–4561.
20. Baish JW, Stylianopoulos T, Lanning RM, et al. Scaling rules for diffusive drug delivery in tumor and normal tissues. *Proc Natl Acad Sci USA.* 2011; 108:1799–1803.